Pertanika J. Sci. & Technol. 34 (5): 2811 - 2833 (2026)

PERTANIKA JOURNALS

SCIENCE & TECHNOLOGY

Journal homepage: http://www.pertanika.upm.edu.my/

# Fractional SIRM Epidemic Model with Microplastic-Mediated Environmental Transmission

**R. Sengothai[1], P. Balaganesan[1]*, D. Adhil Basha[1], and J. Renuka[2]**

*[1]Department of Mathematics, Academy of Maritime Education and Training (AMET University), 135 East Coast Road, Kanathur, Chennai 603112, Tamil Nadu, India*

*[2]Department of Mathematics, Women's Christian College, 51 College Road, Nungambakkam, Chennai 600006, Tamil Nadu, India*

## ABSTRACT

The presence of microplastic particles in terrestrial, marine, and atmospheric systems has made microplastic contamination a serious environmental problem. In addition to their environmental effects, microplastics may serve as carriers of microbial populations, including potentially dangerous pathogens, raising concerns about their contribution to the spread of illness. This work examines the impacts of microplastic-mediated environmental transmission on the dynamics of infectious diseases using a fractional-order SIRM epidemic model. Both direct human-to-human transmission and indirect transmission via contaminated microplastic surfaces are considered in the model. Additionally, it has a unique environmental section that depicts infections associated with microplastic particles. Caputo fractional derivatives are used in the model to represent memory effects that are commonly observed in real epidemiological processes. The basic reproduction number is computed using the next-generation matrix technique, and analytical results show that the solutions are positive and bounded. Sensitivity analysis is used to identify key parameters that influence the spread of illness, and stability analysis of the endemic and disease-free equilibria is performed. Numerical simulations show that microplastic-mediated transmission can substantially increase infection levels and prolong outbreak duration. Overall, the suggested model emphasises the importance of accounting for microplastic contamination in epidemiological investigations and offers a useful framework for understanding the relationship between environmental pollution and infectious disease dynamics.

*Keywords:* Caputo fractional derivative, disease-free equilibrium, epidemic model, infectious disease, microplastic contamination, next-generation matrix, SIRM model, stability analysis

ARTICLE INFO

*Article history:*
Received: 09 July 2026
Accepted: 17 September 2026
Published: 30 October 2026

DOI: https://doi.org/10.47836/pjst.34.5.12

*E-mail addresses*:
kothairam4555@gmail.com (R. Sengothai)
balaganesanpp@gmail.com (P. Balaganesan)
adhilbasha88@gmail.com (D. Adhil Basha)
renukajjm@gmail.com (J. Renuka)
* Corresponding author

e-ISSN: 2231-8526

© Universiti Putra Malaysia Press

## INTRODUCTION

A major global public health concern in recent years has been the emergence of infectious diseases at the human environment interface (Rajkumar, 2022). While previous epidemiological research has mainly focused on direct human-to-human transmission or vector-borne processes, the importance of environmental reservoirs in maintaining pathogen populations is currently garnering greater attention (Asamoah et al., 2022). These reservoirs, which include polluted water, soil, and artificial surfaces, can influence the transmission of illness even without direct contact with affected people.

Because of its persistence and widespread distribution, microplastic contamination has attracted considerable attention among today's environmental issues. Microplastics are tiny plastic particles, usually less than 5 mm, that come from manufactured items like microbeads used in cosmetics and industry, or from the degradation of larger plastic materials (Ding et al., 2023). These particles are now present in freshwater systems, oceans, agricultural soils, and even the atmosphere due to their small size and resistance to degradation (Wu et al., 2023). Global plastic manufacturing has grown dramatically in recent years, according to recent studies, which raises questions about the long-term effects on the environment (Rajkumar, 2022).

Beyond their environmental effects, microplastic particles can act as substrates for microbial colonisation. These surfaces support complex microbial communities, commonly referred to as the plastisphere, which may include opportunistic and potentially pathogenic organisms (Oberbeckmann & Labrenz, 2020). The ability of microplastics to transport such microorganisms across different environments further increases the risk of exposure and transmission over large spatial scales (Wu et al., 2023).

The widespread presence of microplastics, therefore, raises concerns that extend beyond pollution alone. Their potential to support and transport pathogens suggests a possible link between microplastic contamination and the transmission of infectious diseases. This motivates the need to investigate how such environmental factors can be incorporated into epidemiological models in a mathematically meaningful framework.

### The Plastisphere as a Pathogen Reservoir

Beyond ecotoxicological effects on invertebrates and vertebrates, microplastic surfaces function as preferential colonisation substrates for complex microbial assemblages, a phenomenon termed the *plastisphere* (Oberbeckmann & Labrenz, 2020). Metagenomic profiling of plastisphere communities consistently identifies opportunistic and potentially pathogenic taxa, including *Vibrio* spp., antibiotic-resistant *Escherichia coli*, *Pseudomonas aeruginosa*, and diverse filamentous fungi (Ding et al., 2023; Oberbeckmann & Labrenz, 2020). The hydrophobic surfaces of polyethene and polystyrene sorb dissolved organic carbon and facilitate inter-species horizontal gene transfer, creating conditions conducive

to the selection and spread of antimicrobial resistance genes (Ding et al., 2023). Crucially, because microplastics are readily advected by riverine and oceanic currents, they may transport viable pathogens over distances of hundreds to thousands of kilometres, effectively decoupling the spatial origin of contamination from the locus of infection risk (Ding et al., 2023; Mwasa & Tchuenche, 2011). Direct experimental evidence for this pathway comes from Ormsby et al. (2024), who showed that toxigenic Vibrio cholerae colonises and persists on plastic waste for at least 14 days before transferring to floodwater at concentrations sufficient to cause human infection, closing the loop between plastic-surface colonisation and human exposure that motivates the environmental compartment M(t) in the present model.

## Mathematical Epidemiology and Environmental Transmission

Mathematical epidemiology provides a principled framework for disentangling competing transmission pathways and identifying threshold conditions governing whether a pathogen can invade and persist in a host population (Asamoah et al., 2022; Baleanu et al., 2022). The classical susceptible–infected–recovered (*SIR*) paradigm of Kermack and McKendrick has been extended in numerous directions to incorporate environmental pathogen reservoirs. Environmental transmission models, such as those in Capone et al. (2013) and Mwasa & Tchuenche (2011), couple human epidemic dynamics with pathogen persistence in environmental reservoirs.

Related frameworks have been developed for cholera (Capone et al., 2013; Mwasa & Tchuenche, 2011) and hepatitis E (Capone et al., 2013). However, none of these models explicitly treats the microplastic particle as the biotic substrate that concentrates pathogens and shields them from inactivation, a mechanistically distinct reservoir with substantially longer pathogen residence times compared with bulk water.

## Fractional-Order Epidemic Models

Integer order ordinary differential equations encode memoryless, Markovian dynamics. This assumption is frequently violated in biological systems exhibiting anomalous diffusion, power-law immune waning, and history-dependent transmission rates (Rihan et al., 2023). Caputo fractional derivatives of order $\alpha \in (0, 1)$ embed a hereditary convolution kernel into the governing equations, allowing the derivative at time $t$ to depend on the entire past trajectory (Baleanu et al., 2022; Ghanbari, 2020). The order parameter $\alpha$ continuously interpolates between purely diffusive dynamics ($\alpha = 1$, integer-order limit) and strongly sub-diffusive behaviour ($\alpha \to 0^{+}$), enabling flexible empirical calibration to incidence time series. Fractional compartmental models have been applied to a range of infectious diseases, including COVID-19 (Ali et al., 2022; Farman et al., 2022), consistently demonstrating greater fidelity to observed epidemic curves than their integer-order counterparts.

## Research Gap and Original Contributions

Although significant progress has been made separately in microplastic research and fractional-order epidemic modelling, the two have rarely been combined, and existing work in each area has distinct limitations relative to the present study. Environmental-transmission models such as those for cholera (Mwasa & Tchuenche, 2011) and generic SEIR reaction–diffusion systems (Capone et al., 2013) couple human dynamics to a pathogen reservoir but treat that reservoir as an undifferentiated medium (water, soil) and use classical integer-order derivatives, so they cannot capture memory-dependent persistence. Baleanu et al. (2022) extend fractional-order modelling to a real cholera outbreak with an environmental compartment, demonstrating the value of the Caputo formulation for reservoir-mediated transmission; however, their reservoir remains a generic aquatic medium, without a mechanism for the substrate-specific protection and transport that distinguishes microplastic particles from bulk water. Rajkumar (2022) raises the conceptual possibility of a microplastic–infectious-disease link but does not develop a transmission model. Based on the literature reviewed in this study, we found very limited work combining (i) a Caputo fractional-order formulation to capture memory effects in reservoir-mediated transmission, with (ii) a microplastic-specific environmental compartment that reflects the plastisphere's role in concentrating pathogens and extending their residence time relative to bulk water or soil (Ding et al., 2023; Oberbeckmann & Labrenz, 2020). The present study develops a fractional-order SIRM model that incorporates microplastic-mediated environmental transmission to address this combined gap. The aim is to better understand how environmental contamination influences disease dynamics.

The main contributions of this work are summarised as follows:

(i) A fractional-order SIRM model is formulated by including a microplastic associated environmental compartment.

(ii) By distinguishing direct and environmental transmission effects, the next-generation matrix approach is used to determine the basic reproduction number.

(iii) Both endemic and disease-free equilibria are subjected to stability analysis.

(iv) Sensitivity analysis is used to pinpoint important factors affecting the spread of disease.

(v) The effects of fractional dynamics and environmental transmission are demonstrated by numerical simulations.

The structure of this paper is as follows. Section 2 describes the proposed model along with the underlying biological assumptions and parameter definitions. The mathematical analysis of the model is presented in Section 3. Section 4 is devoted to sensitivity analysis, while numerical simulations are discussed in Section 5. The results are further interpreted and compared with existing studies in Section 6. Finally, Section 7 concludes the paper and outlines possible directions for future work.

**Caputo Fractional Derivative**

We employ the Caputo fractional derivative of order $\alpha \in (0, 1]$, defined for a continuous function $f : [0, \infty) \rightarrow \mathbb{R}$ as

$$c_{D^\alpha} f(t) = \frac{1}{\Gamma(1-\alpha)} \int_0^t (t-\tau)^{-\alpha} f'(\tau) d\tau, \quad 0 < \alpha \leq 1, \qquad [1]$$

where $\Gamma(\cdot)$ is the Euler gamma function (Baleanu et al., 2022). At $\alpha = 1$, Equation 1 reduces to the classical first-order derivative. The Caputo formulation is preferred over the Riemann–Liouville derivative in biological modelling because it admits conventional integer-order initial conditions (Ghanbari, 2020).

**Compartmental Structure and Biological Assumptions**

The host population at time *t* is partitioned into:
*S(t)*: **Susceptible** individuals, at risk of acquiring infection.
*I(t)*: **Infected** individuals, actively infectious and shedding pathogens.
*R(t)*: **Recovered** individuals, temporarily immune.

The total living population is $N(t) = S(t) + I(t) + R(t)$. The environmental state variable *M(t)*: Concentration of viable pathogens adsorbed onto microplastic particles (illustratively, cells·mL$^{-1}$) couples the abiotic environment to the human epidemiological system. With M(t) expressed in these units, $\beta_m$ and $\xi$ are reported in the conventional epidemiological units $mL \cdot cells^{-1} \cdot day^{-1}$ *and* $cells \cdot mL^{-1} \cdot person^{-1} \cdot day^{-1}$ respectively (Table 1). These are the ordinary (integer-order) units used for numerical interpretation of the rate coefficients; we do not claim strict dimensional homogeneity of the fractional-order system in the sense of fractional-adjusted units (e.g. $day^{-\alpha}$), which would require a separate convention applied uniformly across all rate parameters.

The model rests on the following biological assumptions:

(A1) New susceptible individuals enter the population at a constant recruitment rate $\Lambda > 0$, while all individuals experience natural mortality at a per-capita rate $\mu > 0$.

(A2) Susceptible individuals acquire infection through direct contact with infectious individuals at a bilinear incidence rate $\beta SI$, where $\beta > 0$ is the effective contact transmission coefficient.

(A3) Susceptible individuals acquire infection through indirect environmental contact with microplastic-borne pathogens at a rate $\beta_m SM$, where $\beta_m > 0$ is the effective microplastic-mediated environmental transmission coefficient, converting exposure to the microplastic-associated pathogen concentration into infection incidence.

(A4) Infected individuals recover at a per-capita rate $\gamma > 0$ and shed pathogens onto microplastic surfaces at a per-capita rate $\xi > 0$.

(A5) Microplastic-associated pathogens are inactivated at a rate $\delta > 0$ via desiccation, ultraviolet radiation, and ecological competition.

(A6) Recovered individuals neither contribute to environmental contamination nor suffer disease-induced mortality on the time scale of interest.

**Compartmental Flow Diagram**

Figure 1 shows a compartmental flow diagram of the fractional-order SIRM epidemic model. Solid arrows represent direct demographic and epidemiological flows. The dashed green arrow represents the indirect environmental transmission pathway mediated by pathogens harboured on microplastic particles.

**Governing Equations**

Based on assumptions (A1) to (A6) and Figure 1, the fractional-order SIRM model is given by the autonomous system in Equations (2a) to (2d):

$$c_D{}^{\propto} S(t) = \Lambda - \beta S(t)I(t) - \beta_{\mathrm{m}} S(t)M(t) - \mu S(t), \quad [2a]$$

$$c_D{}^{\propto} I(t) = \beta S(t)I(t) + \beta_{\mathrm{m}} S(t)M(t) - (\gamma + \mu)I(t), \quad [2b]$$

$$c_D{}^{\propto} R(t) = \gamma I(t) - \mu R(t), \quad [2c]$$

$$c_D{}^{\propto} M(t) = \xi I(t) - \delta M(t), \quad [2d]$$

where $0 < \alpha \leq 1$, supplemented by non-negative initial conditions as shown in Equation 3.

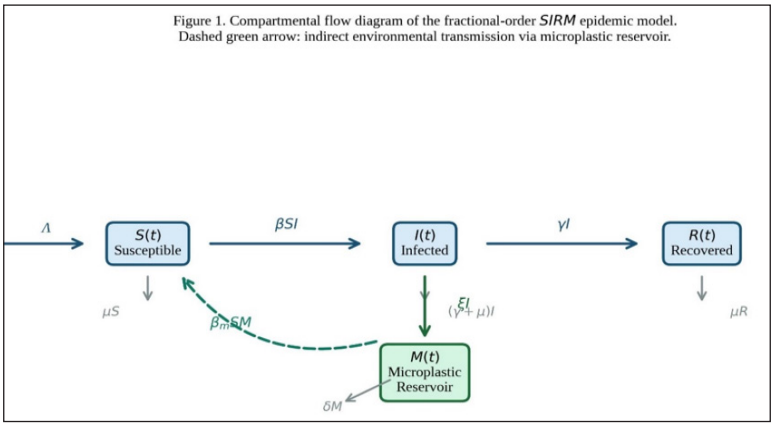


*Figure 1.* Compartmental flow diagram of the fractional-order *SIRM* epidemic model

$$S(0) = S_0 > 0, I(0) = I_0 \geq 0, R(0) = R_0 \geq 0, M(0) = M_0 \geq 0 \quad [3]$$

**Parameter Descriptions and Baseline Values**

The environmental transmission parameter, $\beta_m$, and the pathogen shedding rate ξ are not directly measurable from epidemiological surveillance. Their baseline values are instead anchored qualitatively to the plastisphere literature: Oberbeckmann and Labrenz (2022) and Ding et al. (2023) document active microbial colonisation of microplastic surfaces and pathogen residence times that are substantially extended relative to bulk water, and Zhang et al. (2022) report elevated pathogen loads on freshwater microplastics. These sources support the qualitative pattern encoded in the model (active colonisation, extended persistence) rather than a specific numerical calibration, so the baseline values in Table 1 should be interpreted as illustrative rather than population calibrated. Section 5 accordingly reports how model outcomes respond across a wide range of $\beta_m$ (a 30-fold sweep, Table 3 and Figure 4) rather than a single point estimate, so that the qualitative conclusions can be assessed for robustness to this parameter uncertainty. The Caputo order α is likewise treated as illustrative and literature-informed rather than fitted; calibrating α to case-level incidence data, once microplastic-exposure time series become available, is identified as a direction for future work.

The pathogen decay rate δ has a more direct empirical anchor: Ormsby et al. (2024) report that toxigenic Vibrio cholerae colonised and persisted on plastic waste for at least 14 days before subsequent transfer to floodwater at concentrations sufficient to cause human infection. Treating this reported persistence window as an approximate indicator of the

Table 1
*Model parameters: biological description, units, baseline values used in numerical simulations, and justification in the literature*

| Symbol | Description | Unit | Baseline | Reference |
|---|---|---|---|---|
| Λ | Susceptible recruitment rate | person's day$^{-1}$ | 10.00 | Delavari et al. (2012) |
| $\beta$ | Direct transmission coefficient | person$^{-1}$ day$^{-1}$ | $7.71\times10^{-4}$ | Delavari et al. (2012) |
| $\beta_m$ | Microplastic transmission coefficient | mL·cells$^{-1}$·day$^{-1}$ | $4.83\times10^{-4}$ | Baleanu et al. (2022); est. |
| γ | Recovery rate | day$^{-1}$ | 0.10 | Delavari et al. (2012) |
| μ | Natural mortality rate | day$^{-1}$ | 0.02 | Delavari et al. (2012) |
| ξ | Pathogen shedding rate to microplastics | cells·mL$^{-1}$·person$^{-1}$·day$^{-1}$ | 0.04 | [22]; est. |
| δ | Pathogen decay rate on microplastics | day$^{-1}$ | 0.15 | Baleanu et al. (2022); Rihan et al. (2023); etc. |
| α | Caputo fractional order | – | 0.85 | Ghanbari (2020); illustrative |

timescale over which the pathogen population on plastic remains substantially viable, the baseline $\delta = 0.15$ day$^{-1}$ used here (corresponding to an e-folding decay time of $\approx 6.7$ days) is of the same order of magnitude as, though somewhat faster than, this reported persistence window; this is consistent with $\delta = 0.15$ day$^{-1}$ being a conservative (i.e., not over-optimistic) baseline for the environmental transmission pathway.

The baseline parameter values are selected based on commonly reported ranges in the epidemiological and environmental literature. Parameters related to microplastic transmission ($\beta_m$, $\xi$) are estimated due to the lack of direct empirical data and are primarily used to illustrate plausible transmission scenarios rather than represent a specific calibrated system.

## MATHEMATICAL ANALYSIS

### Positivity of Solutions

**Theorem 3.1** (non-negativity). *For any initial data satisfying (3), the solution* $(S(t), I(t), R(t), M(t))$ *of system (2) satisfies* $(S(t), I(t), R(t), M(t) \geq 0$ *for all* $\geq 0$.

*Proof.* We apply the fractional non-negativity criterion: if $c_D{}^{\propto} x|_{x=0} \geq 0$ and $x(0) \geq 0$, then $x(t) \geq 0$ for all $t \geq 0$ (Li et al., 2019).

**Susceptible class.** At the boundary $S = 0$:

$c_D{}^{\propto} S|_{s=0} = \Lambda > 0$.

Hence $S(t)$ cannot become negative.

**Infected class.** At $I = 0$:

$c_D{}^{\propto} I|_{I=0} = \beta_m S(t) M(t) \geq 0$, since $S, M \geq 0$ by their respective boundary arguments.

**Recovered class.** At $R = 0$:

$c_D{}^{\propto} R|_{R=0} = \gamma I(t) \geq 0$.

**Environmental compartment.** At $M = 0$:

$c_D{}^{\propto} M|_{M=0} = \xi I(t) \geq 0$.

All four state variables satisfy the non-negativity criterion, so the positive orthant $\mathbb{R}^4_+$ is positively invariant under the flow of system (2).

### Uniform Boundedness

**Theorem 3.2** (Uniform boundedness). *Every solution of system (2) originating in* $\mathbb{R}^4_+$ *is uniformly bounded and ultimately confined to the compact absorbing set.*

$$\Omega = \left\{(S, I, R, M) \in \mathbb{R}^4_+ : N(t) \leq \frac{\Lambda}{\mu}, M(t) \leq \frac{\xi\Lambda}{\mu\delta}\right\}.$$

*Proof.* (For initial conditions satisfying $N(0) \leq \Lambda/\mu$ and $M(0) \leq \xi\Lambda/(\mu\delta)$, the set $\Omega$ is positively invariant; for arbitrary nonnegative initial data, solutions remain uniformly bounded and approach these bounds asymptotically, as established below.) Define $N(t) = S(t) + I(t) + R(t)$. Summing Equations (2a)–(2c), we obtain Equation 4:

$$c_{D^\alpha} N(t) = \Lambda - \mu N(t). \quad [4]$$

By the fractional comparison principle (Li et al., 2019):

$$N(t) \leq \left(N(0) - \frac{\Lambda}{\mu}\right) E_\alpha(-\mu t^\alpha) + \frac{\Lambda}{\mu},$$

where $E_\alpha(\cdot)$ is the one-parameter Mittag-Leffler function. Since $E_\alpha(-\mu t^\alpha) \to 0$ as $t \to \infty$ (Li et al., 2019), We obtain lim $sup_{t\to\infty} N(t) \leq \frac{\Lambda}{\mu}$.

For the environmental compartment, equation (2d) yields $c_{D^\alpha} M \leq \xi\Lambda/\mu - \delta M$, giving lim $sup_{t\to\infty} M(t) \leq \xi\Lambda/(\mu\delta)$ by the same argument. Therefore, $\Omega$ is a compact, positively invariant, absorbing set.

**Disease-Free Equilibrium**

At the disease-free equilibrium (DFE) $\varepsilon_0$, The disease is absent $I^* = M^* = 0$. Setting the right-hand sides of Equation (2) to zero and solving, we obtain the disease-free equilibrium given in Equation 5:

$$\varepsilon_0 = \left(\frac{\Lambda}{\mu}, 0, 0, 0\right) \quad [5]$$

This state represents a fully susceptible population free of infection and environmental contamination.

**Basic Reproduction Number via the Next-Generation Matrix**

**Theorem 3.3** (Basic reproduction number). The basic reproduction number of system (2), derived by the next-generation matrix method (van den Driessche, 2017), is given by Equation 6:

$$R_0 = \frac{\beta\Lambda}{\mu(\gamma+\mu)} + \frac{\beta_m\xi\Lambda}{\mu\delta(\gamma+\mu)}, \quad [6]$$

where $R_0^d = \frac{\beta\Lambda}{\mu(\gamma+\mu)}$ is the direct transmission component and $R_0^e = \frac{\beta_m \xi\Lambda}{\mu\delta(\gamma+\mu)}$ is the microplastic-mediated environmental transmission component.

*Proof.* The infected sub-system comprises compartments I and M. Writing $X = (I, M)^T$, the new infection matrix $F$ and the transition matrix $V$ evaluated at $\varepsilon_0 = (S^*, 0, 0, 0), S^* = \frac{\Lambda}{\mu}$, are given in Equation 7.

$$F = \begin{pmatrix} \beta S^* & \beta_m S^* \\ 0 & 0 \end{pmatrix}, \qquad V = \begin{pmatrix} \gamma+\mu & 0 \\ -\xi & \delta \end{pmatrix} \quad [7]$$

The inverse of V is given in Equation 8.

$$V^{-1} = \frac{1}{\delta(\gamma+\mu)} \begin{pmatrix} \delta & 0 \\ \xi & \gamma+\mu \end{pmatrix} \quad [8]$$

The next-generation matrix is given in Equation 9:

$$K = FV^{-1} = \frac{S^*}{\delta(\gamma+\mu)} \begin{pmatrix} \beta\delta + \beta_m \xi & \beta_m(\gamma+\mu) \\ 0 & 0 \end{pmatrix} \quad [9]$$

The spectral radius $R_0 = \rho(K)$ is the single non-zero eigenvalue, yielding expression (6). Since $R_0^e > 0$ whenever $\beta_m, \xi > 0$. The microplastic reservoir always amplifies beyond the direct-contact-only baseline $R_0^d$.

**Local Stability of the Disease-Free Equilibrium**

**Theorem 3.4** (LAS of the DFE). The disease-free equilibrium $E_0$ of system (2) is locally asymptotically stable (LAS) if $R_0 < 1$, and unstable if $R_0 > 1$.

*Proof.* The Jacobian of system (2) at $\varepsilon_0$ is given in Equation 10:

$$J(\varepsilon_0) = \begin{pmatrix} -\mu & \beta S^* & 0 & -\beta_m S^* \\ 0 & \beta S^* - (\gamma+\mu) & 0 & \beta_m S^* \\ 0 & \gamma & -\mu & 0 \\ 0 & \xi & 0 & -\delta \end{pmatrix} \quad [10]$$

Two eigenvalues are evident: $\lambda_1 = \lambda_3 = -\mu < 0$. The remaining pair is determined by the reduced 2 × 2 sub-matrix

$$J_r = \begin{pmatrix} \beta S^* - (\gamma+\mu) & \beta_m S^* \\ \xi & -\delta \end{pmatrix}$$

The characteristic polynomial $p(\lambda) = \lambda^2 - tr(J_r)\lambda + det(J_r)$ has coefficients:

$$tr(J_r) = \beta S^* - (\gamma + \mu + \delta);$$

$$det(J_r) = \delta(\gamma + \mu)(1 - R_0).$$

When $R_0 < 1$: $det(J_r) > 0, and\ tr(J_r) < 0$ (since $\beta S^* = (\gamma + \mu)R_0^d < (\gamma + \mu)$ when $R_0 < 1$). The Routh–Hurwitz criterion guarantees both eigenvalues of $J_r$ have negative real parts. For fractional-order systems, LAS requires for all eigenvalues (Delavari et al., 2012). Because all eigenvalues here are real and negative,

$|arg(\lambda_i)| = \pi > \alpha\pi/2$ for any $\alpha \in (0, 1]$. Hence, $E_0$ is LAS when $R_0 < 1$. When $R_0 > 1$: $det(J_r) < 0$, guaranteeing one positive real eigenvalue, so is unstable.

**Existence and Uniqueness of the Endemic Equilibrium**

**Theorem 3.5** (Endemic equilibrium). System (2) admits a unique endemic equilibrium $E^* = (S^*, I^*, R^*, M^*) \in \text{int}(\Omega)$ with $I^* > 0$ if and only if $R_0 > 1$.

*Proof.* Setting $c_{D^\alpha} M = 0$ in (2d): $M^* = \xi I^*/\delta$. For $I^* > 0$, equation (2b) at steady state gives $S^*(\beta + \beta_m \xi/\delta) = \gamma + \mu$, hence

$$S^* = \frac{\delta(\gamma + \mu)}{\beta\delta + \beta_m \xi}.$$

Then, since at equilibrium $\Lambda = \mu S^* + (\gamma + \mu) I^*$ (obtained by summing (2a) and (2b) at steady state), Substituting S* above and solving for I* gives Equation 11:

$$I^* = \frac{\mu\delta(R_0 - 1)}{\beta\delta + \beta_m \xi} \qquad [11]$$

which is strictly positive if and only if $R_0 > 1$. The remaining components follow: , $R^* = \gamma I^*/\mu, M^* = \xi I^*/\delta, and\ S^* > 0$.

**Theorem 3.6** (LAS of the endemic equilibrium). *If $R_0 > 1$, the endemic equilibrium $E^*$ of system (2) is locally asymptotically stable, for every fractional order $\alpha \in (0, 1]$.*

*Proof.* Since the R-equation decouples from $(S, I, M)$ and contributes only the eigenvalue $-\mu < 0$, it suffices to analyse the reduced $(S, I, M)$-subsystem. Let $\lambda^* = \beta I^* + \beta_m M^*$ denote the force of infection at $E^*$; the equilibrium condition from (2b) gives $\lambda^* S^* = (\gamma + \mu) I^*$. Define the positive constant $q = \frac{\beta_m \xi S^*}{\delta}$ (using $M^* = \frac{\xi I^*}{\delta}$). Linearising (2a), (2b), (2d) at $E^*$, and using $\beta S^* - (\gamma + \mu) = -q$ (obtained by substituting $\lambda^*$ into the equilibrium relation), gives the Jacobian

$$J(E^*) = \begin{bmatrix} -(\lambda^* + \mu) & -\beta S^* & -\beta_m S^* \\ \lambda^* & -q & \beta_m S^* \\ 0 & \xi & -\delta \end{bmatrix}$$

whose characteristic polynomial $s^3 + a_1 s^2 + a_2 s + a_3$ has coefficients (after simplifying using $M^* = \xi I^*/\delta$):

$$a_1 = \delta + \lambda^* + \mu + q,\ a_2 = \beta S^* \lambda^* + \delta\lambda^* + \delta\mu + \lambda^* q + \mu q,\ a_3 = \delta\lambda^*(\beta S^* + q)$$

Since $R_0 > 1$ implies $I^* > 0$ and hence $\lambda^* > 0$, and all model parameters are strictly positive, every term in $a_1$, $a_2$, $a_3$ is a product of positive quantities: $a_1 > 0$ and $a_3 > 0$ follow immediately. Expanding $a_1 a_2 - a_3$ yields

$$a_1 a_2 - a_3 = \beta S^* \lambda^{*2} + \beta S^* \lambda^* \mu + \beta S^* \lambda^* q + \delta^2 \lambda^* + \delta^2 \mu + \delta \lambda^{*2} + 2\delta\lambda^* \mu + \delta\lambda^* q + \delta\mu^2 + 2\delta\mu q + \lambda^{*2} q + 2\lambda^* \mu q + \lambda^* q^2 + \mu^2 q + \mu q^2,$$

a sum of strictly positive terms, so $a_1 a_2 > a_3$. By the Routh–Hurwitz criterion, all three eigenvalues of $J(E^*)$ have a negative real part. Following the same fractional-stability argument as Theorem 3.4 (Delavari et al., 2012), $|arg(\lambda_i)| > \pi/2 \geq \alpha\pi/2$ holds for every $\alpha \in (0,1]$, so $E^*$ is locally asymptotically stable whenever $R_0 < 1$, independent of the fractional order.

## Global Stability of the Disease-Free Equilibrium

**Theorem 3.7** (GAS of the DFE). *If $R_0 < 1$, the disease-free equilibrium $\varepsilon_0$ is globally asymptotically stable in $\Omega$.*

*Proof.* Define the Lyapunov function

$$V(t) = I(t) + \frac{\beta_m S^*}{\delta} M(t) \geq 0, V = 0 \Leftrightarrow I = M = 0$$

Since V is a linear combination of the state variables and the Caputo derivative is a linear operator, $c_{D^\alpha} V = c_{D^\alpha} I + \left(\frac{\beta_m S^*}{\delta}\right) c_{D^\alpha} M$ holds exactly, with no additional regularity condition required. Substituting the governing Equations (2b) and (2d):

$$\begin{aligned} {}^{C}D^{\alpha} V &= \big(\beta S - (\gamma + \mu)\big) I + \beta_m S M + \tfrac{\beta_m S^*}{\delta}(\xi I - \delta M) \\ &= \left(\beta S - (\gamma + \mu) + \tfrac{\beta_m S^*}{\delta}\right) I + \beta_m (S - S^*) M \end{aligned}$$

Since $S \leq S^*$ in $\Omega$, the term $\beta_m(S - S^*)M \leq 0$, Moreover$\beta S \leq \beta S^*$, so ${}^{C}D^{\alpha}V \leq (\gamma + \mu)(R_0 - 1)I \leq 0$ when $R_0 < 1$

For $R_0 < 1, c_{D^{\alpha}}V \leq 0$. The largest invariant subset of the set where $c_{D^{\alpha}}V = 0$ is the disease-free equilibrium $\varepsilon_0$. Indeed, invariance requires $I = 0$; if $M > 0$, Equation (2b) gives $c_{D^{\alpha}}I = \beta_m SM > 0$, so the trajectory leaves the zero-derivative set. Hence $M = 0$, after which $R(t) \to 0$ and $S(t) \to \Lambda/\mu$. By the fractional-order LaSalle invariance principle for Volterra-type Lyapunov functions (Vargas-De-León, 2015), all trajectories in $\Omega$ therefore converge to $\varepsilon_0$, so $\varepsilon_0$ is globally asymptotically stable.

## SENSITIVITY ANALYSIS OF $R_0$

The normalised forward sensitivity index of $R_0$with respect to a parameter $p$ quantifies the fractional change in $R_0$ per unit fractional change in $p$ (Omame et al., 2021):

$$\Upsilon_p^{R_0} = \frac{\partial R_0}{\partial p} \cdot \frac{p}{R_0} \qquad [12]$$

Using expression (6), the analytical sensitivity indices are evaluated at the baseline parameters in Table 1 (where $R_0^d/R_0 \approx 0.857$ and $R_0^e/R_0 \approx 0.143$). Table 2 shows a normalised forward sensitivity indices of $R_0$ evaluated at baseline parameter values (Table 1). A positive (negative) index means that increasing the parameter increases (decreases) $R_0$; the magnitude indicates the proportional impact.

The indices show that $\mu, \Lambda, \gamma$, and $\beta$. These are the highest-leverage parameters. Among the microplastic-specific parameters, $\beta_m$ and $\xi$ carry equal positive indices of 0.143: a 10% increase in either raises $R_0$ by approximately 1.43%. The pathogen decay rate $\delta$ carries an equal but negative index, confirming that accelerating inactivation of microplastic-associated pathogens is a valid, though secondary, intervention strategy.

Table 2
*Normalised forward sensitivity indices of $R_0$ evaluated at baseline parameter values (Table 1)*

| Parameter | Description | Index $\Upsilon_{P_0}$ | Epidemiological Impact |
|---|---|---|---|
| $\Lambda$ | Recruitment rate | +1.000 | Highest amplifier |
| $\beta$ | Direct transmission | +0.857 | High amplifier |
| $\beta_m$ | Environmental transmission | +0.143 | Moderate amplifier |
| $\xi$ | Pathogen shedding | +0.143 | Moderate amplifier |
| $\mu$ | Natural mortality | −1.167 | Highest reducer |
| $\gamma$ | Recovery rate | −0.833 | High reducer |
| $\delta$ | Pathogen decay | −0.143 | Moderate reducer |

It should be noted that the baseline parameter values used in the numerical simulations are selected to illustrate the qualitative dynamics of the proposed model rather than to represent a calibrated fit to a specific epidemiological dataset. Several parameters related to environmental transmission, including the microplastic transmission coefficient $\beta_m$ and the pathogen shedding rate $\xi$ are estimated based on available microbiological studies of microplastic-associated microbial colonisation. The direct transmission coefficient $\beta$ is adopted from commonly used ranges for epidemic modelling in the literature. The numerical experiments are therefore intended to demonstrate the qualitative influence of fractional memory effects and microplastic-mediated environmental transmission on epidemic dynamics.

## NUMERICAL SIMULATION

### Numerical Method

System (2) is integrated numerically using the Adams–Bashforth–Moulton (ABM) predictor-corrector algorithm for Caputo fractional differential equations (Diethelm, Ford & Freed, 2002). The ABM scheme achieves convergence of order 1 + α (Diethelm, Ford & Freed, 2002). Our implementation of the Diethelm-Ford-Freed predictor-corrector scheme was independently validated against the exact Mittag-Leffler solution of the linear test equation $D^{\alpha} y = -y$, $y(0) = 1$, confirming correct convergence prior to application to system (2). All parameter values and initial conditions reported in Table 1 and below were used directly to generate every figure and table in this section, so that $R_0$ computed from equation (6) and $R_0$ realised in the simulations coincide exactly. All computations use step size h = 0.1 days over a simulation horizon of T = 200 days, with baseline parameters from Table 1 and initial conditions:

$$S(0) = 490,\ I(0) = 10,\ R(0) = 0,\ M(0) = 0$$

This initial condition represents the onset of an outbreak from a small, infected seed introduced into an otherwise disease-free population already at its demographic equilibrium, $N(0) = \Lambda/\mu = 500$, with no prior environmental contamination.

### Baseline Epidemic Dynamics $R_0 \approx 3.75$

Figure 2 shows the temporal evolution of all four compartments under baseline parameters, corresponding to an endemic scenario ($R_0 \approx 3.75 > 1$). The susceptible population declines steeply during the exponential growth phase. The infected class reaches its peak around day 23, with about 184 people, then declines as the number of people who can get sick decreases and people keep getting better. The recovered class rises steadily until it reaches

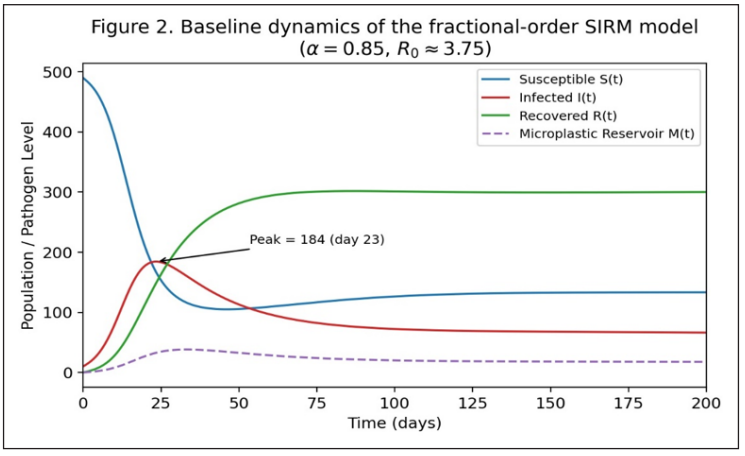


*Figure 2.* Temporal dynamics of all four compartments under baseline parameter values (Table 1) with fractional order α = 0.85. The infected population peaks near day 23 at approximately 184 individuals, while the microplastic reservoir $M(t)$ tracks the infected class with a short lag

its maximum level. The microplastic reservoir $M(t)$ follows $I(t)$. With a short delay, which shows the balance between shedding and decay at the moment in equation (2d).

## Effect of Fractional Order α

Figure 3 shows how the fractional order α affects the spread of infections. As α decreases from 1.0 to 0.75, the infection peak slightly lowers in height, and the epidemic tail gets longer. This is because sub-integer Caputo derivatives encode sub-diffusive memory. When $\alpha = 1.0$, the system becomes the traditional integer-order SIRM model.

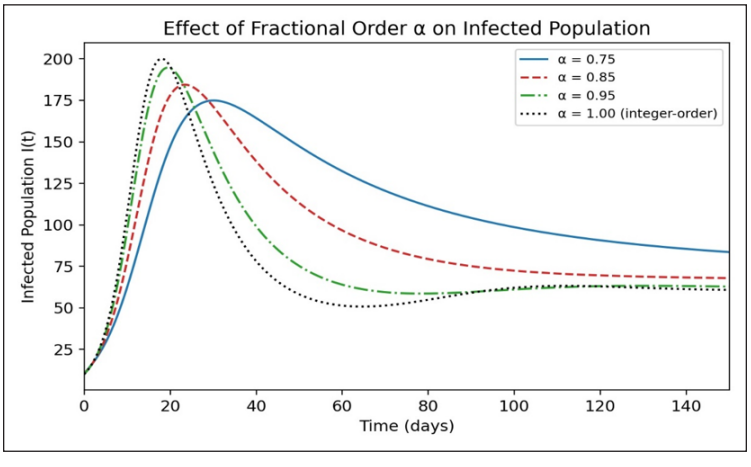


*Figure 3.* Effect of the Caputo fractional order $\alpha$ on the infected population dynamics. Decreasing α modestly reduces the infection peak and broadens the epidemic tail, consistent with the sub-diffusive memory effects encoded by the Caputo derivative. At $\alpha = 1.0$, the model reduces to the classical integer-order SIRM system

### Effect of Microplastic Transmission Rate $\beta_m$

Figure 4 shows how the microplastic transmission coefficient $\beta_m$ affects the spread of disease. When $\beta_m$ goes up from $1 \times 10^{-4}$ to $3 \times 10^{-3}$. The peak of the infection goes up from about 174 to 231 people and moves forward in time. This quantifies the epidemiological cost of environmental microplastic contamination: increasing $\beta_m$ produces a substantial rise in the infection peak.

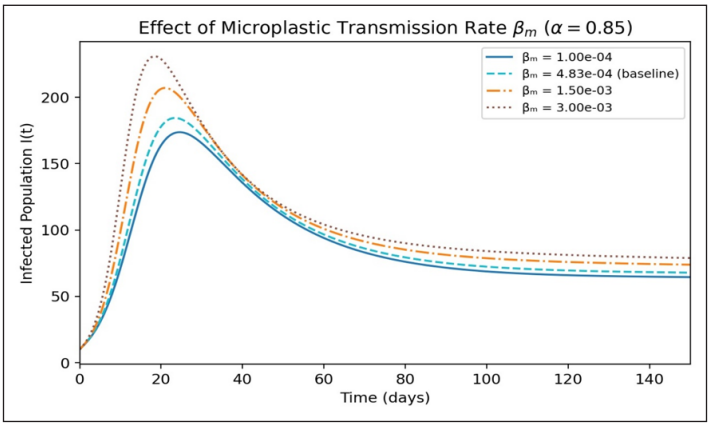


*Figure 4.* Effect of the microplastic-mediated transmission rate $\beta_m$ on the infected population ($\alpha = 0.85$ all other parameters at baseline). Higher $\beta_m$ elevates the peak infected population and prolongs the outbreak, quantifying the epidemiological amplification attributable to the environmental microplastic reservoir

### Phase-Plane Analysis

Figure 5 shows phase portraits in the $S - I$ plane for three different values of α. For $R_0 \approx 3.75 > 1$, all trajectories spiral toward the endemic equilibrium EE, irrespective of α, thereby

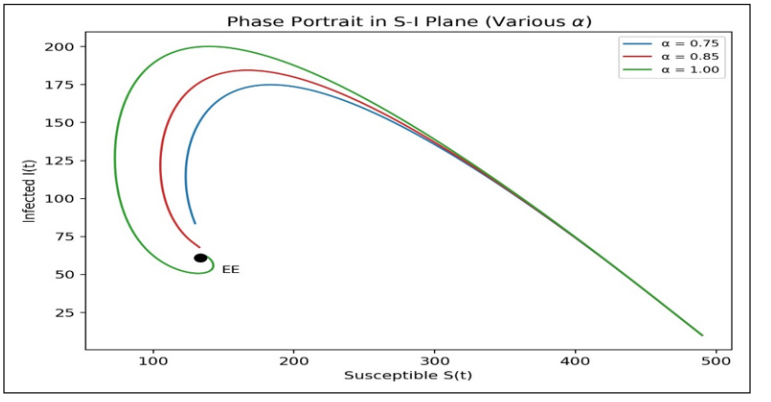


*Figure 5.* Phase portrait in the $S - I$ plane for $\alpha \in \{0.75, 0.85, 1.00\}$ with $R_0 \approx 3.75 > 1$. All trajectories converge to the endemic equilibrium EE, confirming Theorem 3.6. The transient path depends weakly on α, with lower α producing a broader approach to EE

validating the LAS result of Theorem 3.6. The spiral's curvature changes with α, which shows how the fractional memory changes the way the system approaches equilibrium.

**Multi-Parameter Uncertainty Analysis**

The single parameter sweeps above vary $\beta_m$ (or α) individually. To assess robustness under simultaneous parameter uncertainty, we conducted a Latin Hypercube Sampling (LHS) analysis over the five parameters most directly tied to model uncertainty ($\beta, \beta_m$, ξ, δ, $\gamma$), each varied independently across ±50% of its baseline value (Table 1), with $N = 1000$ samples. For each sample, we computed $R_0$ from equation (6), and for a subsample of $N = 200$. We additionally solved the full fractional system (2) to obtain the peak infected population I_max. Partial rank correlation coefficients (PRCCs) were then computed for each parameter between each output, holding the others constant in rank.

Figure 6 presents the partial rank correlation coefficients (PRCCs) for the basic reproduction number $R_0$ and the peak infected population $I_{max}$ under simultaneous parameter uncertainty. Across the LHS ensemble, $R_0$ ranged from 1.40 to 9.08 (mean 4.05), and I_max ranged from 34 to 314 (mean 186), confirming that the baseline qualitative conclusions are not an artefact of the specific point-estimate parameter values. $\beta$ and $\gamma$ dominate both outputs $(|PRCC| > 0.95)$, consistent with the analytical sensitivity indices in Table 2, while $\beta_m$, ξ, and δ each retains a moderate, statistically distinguishable influence $(|PRCC| \approx 0.2 - 0.5)$, confirming that the microplastic-specific pathway remains a non-negligible driver of both threshold behaviour and outbreak severity even after accounting for uncertainty in the other parameters.

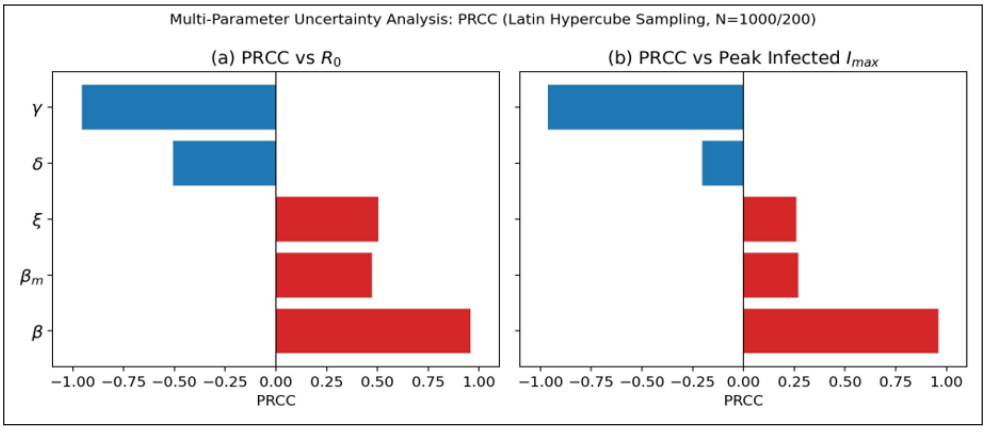


*Figure 6.* Partial rank correlation coefficients (PRCC) between each of the five varied parameters and (a) $R_0$, (b) the peak infected population I_max, under Latin Hypercube Sampling ($N = 1000\ for\ R_0, N = 200$) with each parameter varied over ±50% of its Table 1 baseline

### Simulation Data Summary

Table 3 presents the simulated infected population I(t) at selected time points for different fractional orders α and microplastic transmission coefficients $\beta_m$, as shown in Figures 3 and 4.

## DISCUSSION

In this study, we developed and analysed a Caputo fractional-order SIRM epidemic model that links human infection dynamics with an environmental reservoir of pathogens carried by microplastic particles. The analytical and numerical results help explain how microplastic-mediated transmission can influence disease spread and persistence.

### Decomposition of $R_0$ and the epidemiological role of microplastics

An important analytical result of this study is the additive decomposition (6) of the basic reproduction number into a direct human-to-human component and a microplastic environmental component $R_0^e$. Under the baseline parameter set, $R_0^e/R_0 \approx 14\%$, which indicates that the environmental pathway makes a non-negligible contribution to transmission. This suggests that even if control measures reduce $R_0^d$ to a lower level, the residual contribution from $R_0^e$ may still support persistence of infection when environmental contamination remains present. Similar concerns have been discussed in studies on environmentally mediated transmission, particularly for water-borne pathogens (Mwasa & Tchuenche, 2011), while recent work has also highlighted the potential role of microplastics

Table 3
*Simulated infected population I(t) at selected time points for varying α (left) and varying $\beta_m$ (right). Baseline parameters from Table 1; values rounded to the nearest integer. These representative trajectories correspond to Figures 3 and 4*

| Day | 0.75 | 0.85 | 0.95 | 1.00 | $1\times10^{-4}$ | $4.83\times10^{-4}$ | $1.5\times10^{-3}$ | $3\times10^{-3}$ |
|---|---|---|---|---|---|---|---|---|
| 0 | 10 | 10 | 10 | 10 | 10 | 10 | 10 | 10 |
| 5 | 29 | 32 | 35 | 37 | 31 | 32 | 36 | 43 |
| 10 | 62 | 78 | 97 | 107 | 71 | 78 | 99 | 130 |
| 15 | 108 | 140 | 171 | 186 | 126 | 140 | 175 | 216 |
| 20 | 147 | 178 | 194 | 195 | 164 | 178 | 206 | 229 |
| 25 | 169 | 183 | 174 | 161 | 174 | 183 | 199 | 207 |
| 30 | 175 | 171 | 144 | 125 | 165 | 171 | 179 | 181 |
| 40 | 164 | 138 | 99 | 78 | 136 | 138 | 141 | 142 |
| 50 | 147 | 113 | 75 | 58 | 111 | 113 | 116 | 118 |
| 60 | 132 | 97 | 64 | 51 | 94 | 97 | 101 | 104 |
| 80 | 111 | 79 | 59 | 55 | 76 | 79 | 85 | 90 |
| 100 | 99 | 72 | 61 | 62 | 69 | 72 | 79 | 84 |

as carriers of pathogenic microorganisms (Ding et al., 2023; Oberbeckmann & Labrenz, 2020; Rajkumar, 2022).

### Epidemiological implications of $\beta_m$ and the shedding rate $\xi$

Sensitivity analysis identifies $\beta_m$ and $\xi$ as the microplastic-specific parameters with the highest leverage on $R_0$, each carrying a normalised index of +0.143. The numerical experiments in Section 5 demonstrate that increasing $\beta_m$ from $1\times10^{-4}$ to $3\times10^{-3}$ increases the infection peak from approximately 174 to 231 individuals, highlighting the amplification of epidemic severity associated with stronger environmental transmission. The epidemiological implications can be interpreted as follows:

In practice, $\beta_m$ may be reduced by limiting plastic waste entering aquatic environments, improving wastewater treatment to remove microplastics, and reducing direct exposure to contaminated water sources (Rajkumar, 2022; Wu et al., 2023). The shedding rate $\xi$ reflects the contribution of infected individuals to environmental contamination, and reducing this parameter may help decrease pathogen accumulation in the microplastic reservoir. The combined effect of $\beta_m$and $\xi$ highlights the importance of environmental control strategies alongside traditional epidemiological interventions.

### Memory effects and the fractional order $\alpha$

The epidemic process's memory is demonstrated by the fractional order $\alpha$. The model assigns greater weight to previous states when $\alpha < 1$. This enables it to explain long-lasting or delayed effects, which are typical in actual transmission dynamics. Reducing $\alpha$ from 1.0 to 0.75 in the current simulations prolongs the epidemic tail and somewhat reduces the infection peak. Studies on COVID-19 and related infectious diseases have shown a similar tendency in other fractional epidemic models (Ali et al., 2022; Farman et al., 2022; Rihan et al., 2023). Estimating $\alpha$ from observed epidemiological data would improve the model's practical relevance and help connect the fractional formulation to measurable outbreak behaviour. Table 3 already provides a direct integer-order comparison, since $\alpha - 1.00$ is the classical integer-order limit of system (2). At the peak (day 20), the fractional-order case $\alpha = 0.75$ predicts $I(20) \approx 147$ versus $I(20) \approx 195$ for the integer-order case $\alpha - 1.00$, a reduction of approximately 25%. More strikingly, the two cases diverge in the opposite direction later: by day 60 the fractional case still shows $I(60) \approx 132$ while the integer-order case has already relaxed to $I(60) \approx 51$ , having passed through a damped oscillation toward the endemic equilibrium (visible in Figure 3). This illustrates concretely how sub-diffusive memory both lowers the initial peak and substantially prolongs the epidemic tail relative to the classical model, rather than merely shifting the curve.

### Comparison with existing frameworks

The present model is related to earlier epidemic models that incorporate environmental transmission, but it differs in several important aspects. First, the environmental compartment in this study explicitly represents pathogens associated with microplastic particles, providing a more direct framework to analyse this emerging transmission pathway (Ding et al., 2023; Oberbeckmann & Labrenz, 2020; Rajkumar, 2022). Second, the model is formulated using Caputo fractional-order derivatives, which allow memory effects to be included in the system dynamics (Ali et al., 2022; Rihan et al., 2023). In contrast to spatial or reaction–diffusion epidemic models (Capone et al., 2013), the present model is spatially homogeneous and is intended to capture population-level behaviour rather than spatial spread.

## LIMITATIONS

Several simplifications warrant acknowledgement. The model assumes homogeneous mixing and neglects age structure, network heterogeneity, and spatial dispersion, all of which demonstrably influence epidemic dynamics. The bilinear incidence $\beta SI$ may overestimate transmission at high prevalence; saturating incidence of Holling type II form $\beta SI/(1 + kI)$ . It is a more realistic alternative. Parameter values for $\beta_m$ and $\xi$ are estimated from the microbiological literature rather than from direct epidemiological fitting, and calibration against field data for a specific pathogen microplastic combination (e.g. *Vibrio cholerae* on polyethene fragments) remains a critical future step. Disease-induced mortality, waning immunity, multiple pathogen serotypes, and seasonal forcing of transmission rates are excluded for analytical tractability.

## CONCLUSION

We have developed and analysed a Caputo fractional-order SIRM model that explicitly incorporates microplastic particles as an environmental reservoir of pathogens. To the best of our knowledge, this is among the early attempts to integrate microplastic-mediated transmission into an epidemic modelling framework. The main findings of this study can be summarised as follows:

(i) The feasible region $\Omega \subset \mathbb{R}^4_+$. It is shown to be compact and positively invariant, and all solutions remain uniformly bounded over time. This confirms that the model is biologically meaningful and mathematically well-posed.

(ii) The basic reproduction number is expressed as $R_0 = R_0^d + R_0^e$, which clearly separates the contributions from direct transmission and environmental transmission. This decomposition indicates that the presence of microplastics consistently increases the overall transmission potential.

(iii) The disease-free equilibrium is globally asymptotically stable when $R_0 < 1$, (Theorem 3.7). A unique endemic equilibrium exists whenever $R_0 > 1$ (Theorem 3.5) and is locally asymptotically stable for every fractional order $\alpha \in (0,1]$ (Theorem 3.6), so local stability of $E^*$ holds unconditionally on parameter values once $R_0 < 1$.

(iv) Sensitivity analysis suggests that the recovery rate $\gamma$, recruitment rate $\Lambda$, and direct transmission coefficient $\beta$ play dominant roles in shaping disease dynamics. In addition, the parameters $\beta_m$ and $\xi$, which are directly associated with microplastic-mediated transmission, appear to be important from a practical intervention perspective.

(v) The numerical simulations support the analytical results and reveal that fractional-order dynamics tend to prolong the persistence of infection. Furthermore, higher values of $\beta_m$ lead to noticeable increases in infection peaks, highlighting the epidemiological importance of environmental contamination.

The results of this work suggest that microplastic pollution may play a non-negligible role in the spread and persistence of infectious diseases. This observation points to the need for integrating environmental control strategies with traditional public health measures. Several possible extensions can be considered in future studies. These include incorporating spatial effects through reaction–diffusion formulations, developing stochastic fractional models to capture uncertainty in small populations, and applying optimal control techniques to balance intervention strategies. Further work may also explore multi-pathogen interactions and validate the model using epidemiological and environmental data.

Overall, the proposed framework provides a useful step toward connecting environmental pollution with infectious disease modelling and opens new directions for interdisciplinary research at the intersection of mathematical epidemiology and environmental science.

## ACKNOWLEDGEMENT

The authors would like to thank the Academy of Maritime Education and Training (AMET University), Chennai, India, for its institutional support.

## REFERENCES

Ali, A., Islam, S., Khan, M. R., Rasheed, S., Allehiany, F. M., Baili, J., Khan, M. A., & Ahmad, H. (2022). Dynamics of a fractional order Zika virus model with mutant. *Alexandria Engineering Journal, 61*(6), 4821-4836. https://doi.org/10.1016/j.aej.2021.10.031

Asamoah, J. K. K., Okyere, E., Abidemi, A., Moore, S. E., Sun, G.-Q., Jin, Z., Acheampong, E., & Gordon, J. F. (2022). Optimal control and comprehensive cost-effectiveness analysis for COVID-19. *Results in Physics, 33*, Article 105177. https://doi.org/10.1016/j.rinp.2022.105177

Baleanu, D., Ghassabzade, F. A., Nieto, J. J., & Jajarmi, A. (2022). On a new and generalized fractional model for a real cholera outbreak. *Alexandria Engineering Journal, 61*(11), 9175-9186. https://doi.org/10.1016/j.aej.2022.02.054

Capone, F., De Cataldis, V., & De Luca, R. (2013). On the nonlinear stability of an epidemic SEIR reaction-diffusion model. *Ricerche di Matematica, 62*(1), 161-181. https://doi.org/10.1007/s11587-013-0151-y

Delavari, H., Baleanu, D., & Sadati, J. (2012). Stability analysis of Caputo fractional-order nonlinear systems revisited. *Nonlinear Dynamics, 67*(4), 2433-2439. https://doi.org/10.1007/s11071-011-0157-5

Diethelm, K., Ford, N. J., & Freed, A. D. (2002). A predictor-corrector approach for the numerical solution of fractional differential equations. *Nonlinear Dynamics, 29*(1-4), 3-22. https://doi.org/10.1023/a:1016592219341

Ding, J., Huang, Z., Liu, C., Li, L., Zhang, S., & Zhu, X. (2023). Microplastics as vectors of pathogenic microorganisms in aquatic environments: Occurrence, mechanisms, and management strategies. *Science of the Total Environment, 880*, Article 163299.

Farman, M., Akgül, A., Nisar, K. S., Ahmad, D., Ahmad, A., Kamangar, S., & Saleel, C. A. (2022). Epidemiological analysis of fractional order COVID-19 model with Mittag-Leffler kernel. *AIMS Mathematics, 7*(1), 756-783. https://doi.org/10.3934/math.2022046

Ghanbari, B. (2020). On the modeling of the interaction between tumor growth and the immune system using some new fractional and fractional-fractal operators. *Advances in Difference Equations, 2020*(1), Article 585. https://doi.org/10.1186/s13662-020-03040-x

Li, H., Cheng, J., Li, H.-B., & Zhong, S.-M. (2019). Stability analysis of a fractional-order linear system described by the Caputo–Fabrizio derivative. *Mathematics, 7*(2), Article 200. https://doi.org/10.3390/math7020200

Mwasa, A., & Tchuenche, J. M. (2011). Mathematical analysis of a cholera model with public health interventions. *Biosystems, 105*(3), 190-200. https://doi.org/10.1016/j.biosystems.2011.04.001

Oberbeckmann, S., & Labrenz, M. (2020). Marine microbial assemblages on microplastics: Diversity, adaptation, and role in degradation. *Annual Review of Marine Science, 12*, 209-232. https://doi.org/10.1146/annurev-marine-010419-010633

Omame, A., Abbas, M., & Onyenegecha, C. P. (2021). A fractional-order model for COVID-19 and tuberculosis co-infection using Atangana–Baleanu derivative. *Chaos, Solitons & Fractals, 153*, Article 111486. https://doi.org/10.1016/j.chaos.2021.111486

Ormsby, M. J., Woodford, L., White, H. L., Fellows, R., Oliver, D. M., & Quilliam, R. S. (2024). Toxigenic Vibrio cholerae can cycle between environmental plastic waste and floodwater: Implications for environmental management of cholera. *Journal of Hazardous Materials, 461*, Article 132492. https://doi.org/10.1016/j.jhazmat.2023.132492

Rajkumar, R. P. (2022). Microplastics and infectious diseases: Is there a link? *Journal of Water and Health, 20*(2), 214-225.

Rihan, F. A., Kandasamy, U., Alsakaji, H. J., & Sottocornola, N. (2023). Dynamics of a fractional-order delayed model of COVID-19 with vaccination efficacy. *Vaccines, 11*(4), Article 758. https://doi.org/10.3390/vaccines11040758

van den Driessche, P. (2017). Reproduction numbers of infectious disease models. *Infectious Disease Modelling, 2*(3), 288-303. https://doi.org/10.1016/j.idm.2017.06.002

Vargas-De-León, C. (2015). Volterra-type Lyapunov functions for fractional-order epidemic systems. *Communications in Nonlinear Science and Numerical Simulation, 24*(1-3), 75-85. https://doi.org/10.1016/j.cnsns.2014.12.013

Wu, P., Huang, Y., Zheng, H., Chen, G., Sun, X., & Cai, Z. (2023). Microplastics in the aquatic environment: Occurrence, fate, environmental risk and management. *Science of the Total Environment, 905*, Article 167028.

Zhang, Y., Lu, X., Liu, W., Li, Z., Yu, H., Cao, G., & Zhao, L. (2022). Microplastic-associated pathogens in freshwater environments: Distribution, interactions and health implications. *Environmental Pollution, 312*, Article 119966.